Journal of Hazardous Materials 185 (2011) 653–661

Contents lists available at ScienceDirect

Journal of Hazardous Materials

journal homepage: www.elsevier.com/locate/jhazmat

Magnetic Fe_2MO_4 (M:Fe, Mn) activated carbons: Fabrication, characterization and heterogeneous Fenton oxidation of methyl orange

Thi Dung Nguyen[a], Ngoc Hoa Phan[b], Manh Huy Do[a,*], Kim Tham Ngo[a,c]

[a] Institute of Chemical Technology, Vietnamese Academy of Science and Technology, 01 Mac Dinh Chi, District 1, Ho Chi Minh, Viet Nam
[b] Department of Chemical Technology, Hochiminh University of Technology, 268 Ly Thuong Kiet, District 10, Ho Chi Minh, Viet Nam
[c] College of science, Can Tho University, 3/2, Can Tho, Viet Nam

ARTICLE INFO

Article history:
Received 29 April 2010
Received in revised form 19 August 2010
Accepted 17 September 2010
Available online 25 September 2010

Keywords:
Degradation
Fenton reaction
Magnetic activated carbon
Methyl orange
Heterogeneous catalysts

ABSTRACT

We present a simple and efficient method for the fabrication of magnetic Fe_2MO_4 (M:Fe and Mn) activated carbons (Fe_2MO_4/AC-H, M:Fe and Mn) by impregnating the activated carbon with simultaneous magnetic precursor and carbon modifying agent followed by calcination. The obtained samples were characterized by nitrogen adsorption isotherms, X-ray diffraction (XRD), scanning electron microscopy (SEM) and vibrating sample magnetometer (VSM), and the catalytic activity in heterogeneous Fenton oxidation of methyl orange (MO) was evaluated. The resulting Fe_2MnO_4/AC-H showed higher catalytic activity in the methyl orange oxidation than Fe_3O_4/AC-H. The effect of operational parameters (pH, catalyst loading H_2O_2 dosage and initial MO concentration) on degradation performance of the oxidation process was investigated. Stability and reusability of selected catalyst were also tested.

1. Introduction

Nowadays, the pollution of water resources by the dyes from the textiles industries has become a serious environmental problem attracting much more attention. Most of the dyes used in the textiles industries are azo dyes with one or more azo bonds (–N=N–) in association with one or more aromatic systems [1]. The removal of azo dyes from wastewater is a challenge to the textiles industries because the azo dyes are difficult to destroy by biological and conventional chemical treatments due to their toxicity and stability. Recently, advanced oxidation processes (AOPs) based on the generation of a free hydroxyl radical ($OH^•$) which degrades most organic pollutants quickly and non-selectively, are reported as a potential alternative for the treatment of industrial wastewater containing non-biodegradable organic pollutants. Among these AOPs, Fenton's Reagent (H_2O_2/Fe^{2+} or Fe^{3+}) seems to be a promising one due to its low cost and environmental benignity. However, the application of Fenton processes based on homogeneous ferrous or ferric salts usually suffers several drawbacks. These include the need of recovering iron after the catalytic treatment, the limited pH range (pH 2–3) and the catalyst deactivation by some iron complexing agents such as phosphate anions and some intermediate oxidation products, etc. [2–5]. To overcome these drawbacks, the heterogeneous catalysts based on incorporating Fenton's catalyst onto surfaces of different supports have been developed and employed. For example, the use of zeolite-immobilized Fe ions [5–11], Fe pillared clay [12–16], or polymer supported Fe [17,18] for the degradation of dyes or other organic compounds. Unfortunately, most of them showed relatively low activities or the requirement of UV light for photocatalysis or strong iron leaching due to low pH and low chemical stability of the supports [19–22].

Recent studies [23–25] have shown that magnetite is the most effective heterogeneous Fenton catalyst compared to other iron oxides, possibly because it is the only one that has Fe^{2+} in its structure, thus enhancing the production rate of $OH^•$ [25]. In addition, Costa et al. [26,27] reported that the introduction of Co and Mn into magnetite structure to form $Fe_{3-x}Co_xO_4$ and $Fe_{3-x}Mn_xO_4$ may strongly promote both the H_2O_2 decomposition and the degradation of organic compounds in an aqueous medium. Due to their low cost, wide availability, high specific surface area and porosity, chemical inertness and thermal stability, activated carbons (ACs) may be good supports for producing this kind of low cost, high performance catalyst. To incorporate magnetic particles on AC, several methods such as high-energy milling [28], reducing [29] and chemical coprecipitation [30–32] have been developed. However, the magnetic activated carbons obtained using these methods are only able to retain a low portion of the porosity of the activated carbon because the pore space of the activated carbon was blocked by the presence of magnetic particles which have a low surface area and microporous volume,

* Corresponding author. Tel.: +84 838256394; fax: +84 838293889.
E-mail address: huydoma@vast-hcm.ac.vn (M.H. Do).

0304-3894/$ – see front matter © 2010 Elsevier B.V. All rights reserved.
doi:10.1016/j.jhazmat.2010.09.068

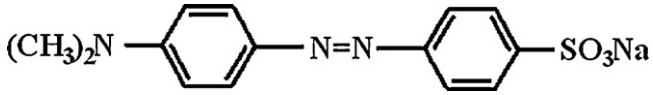

Fig. 1. Chemical structure of methyl orange.

whereas the new pore structures of the activated carbon were not built.

Herein, in the present work we report a novel and simple method for fabricating magnetic Fe_2MO_4 (M:Fe, Mn) activated carbons with high retained porosity. This method involves first impregnating commercial activated carbons with a solution mixture containing magnetic precursors ($Fe(NO_3)_3{\cdot}9H_2O$ or $Fe(NO_3)_3{\cdot}9H_2O$ and $MnSO_4{\cdot}H_2O$) and a carbon modifying agent (HNO_3 20%). The impregnated activated carbons were then dried and calcined to form the magnetic Fe_2MO_4 (M:Fe, Mn) particles. The catalytic effect of the obtained magnetic activated carbons was investigated in the Fenton oxidation of MO. Stability and reusability of the Fe_2MnO_4/AC-H were also tested.

2. Experimental

2.1. Materials

Commercial coconut shell based activated carbon was provided by Tra Vinh, Viet Nam. The activated carbon was sifted to 50–60 meshes before being used. For impregnating activated carbons, $MnSO_4{\cdot}H_2O$ and $Fe(NO_3)_3{\cdot}9H_2O$ (obtained from Xilong Chemical Factory, Quangdong) were employed as the magnetic precursors. Nitric acid (HNO_3 65%), which was used as a carbon modifying agent, was purchased from Merck. For the Fenton oxidation, MO was chosen as the model organic pollutant. The structure of the dye is presented in Fig. 1. Hydrogen peroxide solution (>30%) used as the Fenton agent was purchased from the Shanghai Chemical Company.

2.2. Fabrication of magnetic activated carbon materials.

First, 20 g activated carbon was impregnated into a 40 mL solution mixture of $Fe(NO_3)_3{\cdot}9H_2O$ (0.25 mol) and HNO_3 (20%) or $Fe(NO_3)_3{\cdot}9H_2O$ (0.17 mol) and $MnSO_4{\cdot}H_2O$ (0.08 mol) and HNO_3 (20%) at room temperature for 24 h. Then, the impregnated activated carbons were filtrated and naturally dried at ambient temperature. Finally, the dried activated carbons were treated at 600 °C for 1 h in the presence of nitrogen to form the magnetic activated carbon materials. The obtained materials are denoted as Fe_3O_4/AC-H and Fe_2MnO_4/AC-H, respectively. The synthesis of a blank AC-H sample followed the same procedure except that the impregnation solution was without the magnetic precursors. The actual Fe and Mn mass contents in the materials were determined in an atomic absorption spectrometer (GBC, Avanta, Australia). The determination result is listed in Table 1.

2.3. Characterization of magnetic activated carbon materials

The XRD measurement was carried out on an XRD diffractometer (D8 Advance, Brucker, Germany). The patterns with the Cu-Kα radiation (λ = 1.54051 Å) at 40 kV and 40 mA were recorded in the region of 2θ from 5° to 75°. Nitrogen adsorption and desorption isotherms were performed at −196 °C in a Brunauer–Emmett–Teller (BET) sorptometer (model: BET 201-A). The BET surface area was deduced by analyzing the isotherm in the relative pressure range of 0.05–0.3. Micropore volume (V_{micro}) was calculated after applying the Dubinin-Radushkevich (DR) equation to the N_2 adsorption isotherm. Total pore volume (V_t) was obtained from the amount adsorbed at a relative pressure of 0.99 and the mesopore volume (V_{meso}) was determined as the difference between these two values. SEM was carried out by means of a Hitachi S-4800 Scanning Electron Microscope (Hitachi Co., Japan). The magnetic properties of the materials were studied with a VSP (PPMS6000, US) at room temperature, and the hysteretic loop was obtained in a magnetic field that varied from −7 T to +7 T. The pH at point of zero charge, pH_{PZC}, was carried out according to the following method. A 0.1 M solution of NaCl was prepared using distilled water, which was degasified by boiling for 30 min. Eleven different standards having pH ranging from 2 to 12 were made using such a solution. 0.5 g of sample was added to 20 mL of each solution, and stirred overnight to reach equilibrium. The final pH was measured, and plotted as a function of the initial pH of the solution. pH_{PZC} was determined as the pH of the NaCl solution that did not change after the contact with the catalyst sample. The result is listed in Table 1.

2.4. Catalytic oxidation of methyl orange by H_2O_2

The heterogeneous Fenton oxidation of MO was carried out in a cylindrical Pyrex vessel (500 mL) placed in a water bath with a magnetic stirrer. The catalyst was introduced into 200 mL methyl orange solution with magnetic-stirring to maintain a uniform suspension. After allowing 15 min for the adsorption/desorption of MO to reach equilibrium, H_2O_2 was added into the reactor and time logged. Throughout the reaction, the reactant solution was adjusted to constant pH with dilute aqueous HCl 0.01 M or NaOH 0.01 M solutions. Samplings were taken at a given time intervals during the reaction. Then samples were analyzed immediately after filtration through 0.2 μm Millipore membrane filters to remove suspended particles. For TOC analysis, all the samples were immediately treated with scavenging reagent (0.1 M Na_2SO_3, 0.1 M KH_2PO_4, 0.1 M KI and 0.05 M NaOH) to obtain accurate TOC values [33].

2.5. Analytical methods

The concentration of MO was analyzed on UV–vis spectrophotometer (UV-1800, Shimadzu, Japan) with its adsorption at 465 nm for samples that had pH > 3 and at 500 nm for samples that had pH ≤ 3. To evaluate the mineralization of the MO, total organic carbon (TOC) was measured using a Shimadzu TOC-V_{CPH} Analyzer. The leaching concentrations of Fe and Mn in the solution were measured by an atomic absorption spectrometer (GBC, Avanta, Australia).

3. Results and discussion

3.1. Characterization of samples

Fig. 2 shows the nitrogen adsorption and desorption isotherms and the pore size distribution (inset) obtained for AC-H, Fe_3O_4/AC-H and Fe_2MnO_4/AC-H. The mesopore and micropore size distributions were calculated using the Dollimore–Heal (DH) and Horvath–Kawazoe (HK) methods. The isotherms exhibit a feature of type H4 hysteresis loop [34], this type of the hysteresis loop is often associated with narrow slit pores and include pores in the micropore region [35]. The DH and HK pore size analysis also shows that for all samples the pore size distribution contains pores in both micropore (<2 nm) and mesopore (2–20 nm) region (see Fig. 2, inset).

The textural characteristics of the ACF-H, Fe_3O_4/AC-H and Fe_2MnO_4/AC-H determined according to the isotherms are given in Table 1. It is noteworthy to mention that in spite of the presence of Fe_3O_4 particles which have a relatively small surface area and pore volume compare to ACs, textural properties of the Fe_3O_4/AC-H including specific surface area and total volume, mesopore and

Table 1
The Fe, Mn contents, textural properties and pH_{PZC} of the samples.

Sample	Fe (wt%)	Mn (wt%)	S_{BET} ($m^2\ g^{-1}$)	V_t ($cm^3\ g^{-1}$)	V_{micro} ($cm^3\ g^{-1}$)	V_{meso} ($cm^3\ g^{-1}$)	pH_{PZC}
AC-H	–	–	919.53	1.0044	0.4759	0.5285	8.0
Fe_3O_4/AC-H	3.120	–	999.68	1.0365	0.5184	0.5181	9.0
Fe_2MnO_4/AC-H	2.647	0.933	806.30	0.8665	0.4150	0.4515	9.9
Fe_3O_4	~72	–	291.30	0.3933	0.1562	0.2371	–
Fe_2MnO_4	~48	~24	82.38	0.3265	0.0434	0.2831	–

micropore is higher than those of AC-H. This is probably due to the oxidation action of Fe(III) salt which plays a role as an activating agent for carbon materials [36–41]. Oliveira et al. [41] found that AC obtained with ferric salt as activating agent shows high specific surface area even at lower activation temperatures (280 °C). Back to Fig. 2 (inset), another observation is that the mesopore size distribution of the Fe_3O_4/AC-H is slightly wider than that of the AC-H, which provides further evidence for the activating role of Fe(III) salt. However, in the case of the Fe_2MnO_4/AC-H, its textural properties slightly decrease. Compared with Fe_3O_4/AC-H, Fe_2MnO_4/AC-H has much lower porosity. This probably has two causes. First, it is attributed to the lower Fe(III) salt amount, leading to the pore space built by the activating agent not being sufficient to cover space blocked by the magnetic Fe_2MnO_4 particles. Second, it is thought as Fe_2MnO_4 particles have much smaller surface area and pore volume compare to Fe_3O_4 particles. The first cause is less likely because the difference in Fe contents of the Fe_3O_4/AC-H and Fe_2MnO_4/AC-H is not significant (less than 5%). To study the second cause, here we prepared Fe_3O_4 and Fe_2MnO_4 powder by using coprecipitation method. 0.2 mol $FeCl_3$ and 0.1 mol $FeCl_2$ or 0.1 mol $MnSO_4$ were dissolved in 100 mL of distilled water. Under vigorous magnetic-stirring, raised the pH by adding 50% NaOH solution to around 11. The suspension was heated at 100 °C for 1 h. The precipitate was washed several times with distilled water and dried in a vacuum oven at 80 °C for 5 h. The dry material was crushed and then calcinated at 350 °C for 1 h. The crystal phase structure of prepared Fe_3O_4 and Fe_2MnO_4 powder was confirmed with XRD analysis (data not shown) and their textural properties were characterized by nitrogen adsorption isotherms. The result is showed in Fig. 2 and Table 1. As expected, Fe_2MnO_4 powder has a relatively small surface area and microporous volume (82.38 $m^2\ g^{-1}$ and 0.0433 $cm^3\ g^{-1}$, respectively), whereas Fe_3O_4 powder has a relatively high surface area and microporous volume (291.30 $m^2\ g^{-1}$ and 0.1562 $cm^3\ g^{-1}$, respectively). Compared with the Fe_3O_4 powder, the surface area of the Fe_2MnO_4 powder was observed to reduce about 71.7%. This value is much higher than the 19.3% value corresponding to reduction of the surface area of the Fe_2MnO_4/AC-H compared with Fe_3O_4/AC-H. This may be due to the difference in Fe/Mn ratio of the Fe_2MnO_4 powder and Fe_2MnO_4/AC-H samples as well as the activating role of Fe(III) salt. The decrease in porosity of the Fe_2MnO_4 powder and Fe_2MnO_4/AC-H may be also due to using $MnSO_4.H_2O$ as the magnetic precursors, lead to the deposit of SO_4^{2-} ions that are not yet removed inside the wormhole channels which would contribute to an increase of skeletal density and a concomitant loss of void space, effectively lowering the surface area per gram. This will be the aim of future work.

Fig. 3 shows XRD patterns for the Fe_3O_4/AC-H and Fe_2MnO_4/AC-H samples. The AC matrix shows, for all samples, an amorphous halo. The formation of the ferrite and manganese ferrite spinels was confirmed from the XRD patterns for Fe_3O_4/AC-H and Fe_2MnO_4/AC-H by comparison with JCPDS files 251402 and 100319 for Fe_3O_4 and Fe_2MnO_4, respectively.

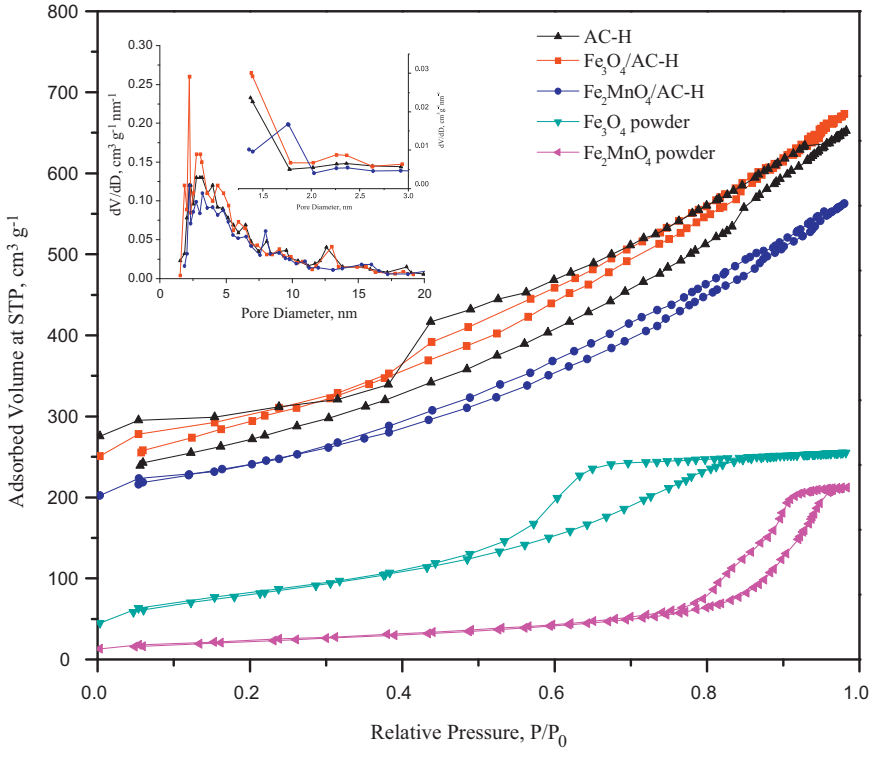

Fig. 2. The nitrogen adsorption–desorption isotherms and pore size distributions (inset) of ACF-H, Fe_3O_4/AC-H and Fe_2MnO_4/AC-H.

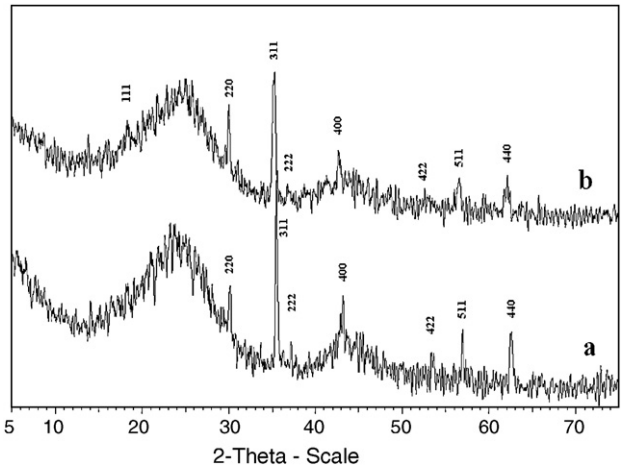

Fig. 3. XRD patterns of (a) Fe_3O_4/AC-H and (b) Fe_2MnO_4/AC-H samples.

The morphology of the samples was investigated by SEM and shown in Fig. 4. It can be seen that the magnetic particles deposited and formed new pores on AC. These pores may be a reason for improving or maintaining the high surface area and porosity of activated carbon in the presence of the Fe_3O_4 or Fe_2MnO_4 particles

Fig. 5 and Table 2 show the room temperature magnetization curves and the magnetization property data of the Fe_3O_4/AC-H and Fe_2MnO_4/AC-H samples. The results obtained show, for both samples, a similar behaviour in magnetic property. The saturation magnetization (Ms), coercive field (Hc) and remanent magnetization (Mr) of both Fe_3O_4/AC-H and Fe_2MnO_4/AC-H are lower than those reported for bare Fe_3O_4 nanoparticles (Ms = 58.94 emu g^{-1}, Hc = 160.1 Oe, Mr = 7.4 emu g^{-1}) [42] and bare Fe_2MnO_4 nanoparticles (Ms = 70 emu g^{-1}, Hc = 200 Oe, Mr = 17 emu g^{-1}) [43]. The decrease could result from the existence of AC and the smaller size of magnetic particles. The lower Hc values imply that they can be separated easily by a magnet or an applied magnetic field. Moreover, after separating, they can be easily re-dispersed in a solution for reuse due to their low Mr values. These results show that the Fe_3O_4/AC-H and Fe_2MnO_4/AC-H materials can be manipulated by an external magnetic field, such as a magnet (Fig. 5, inset), thus providing a potential advantage for the separation, recovery and reuse of catalysts.

3.2. Degradation of MO by Fe_2MO_4/AC-H

First, the influence of the adsorption processes was determined in experiments carried out without H_2O_2. As shown in Fig. 6, the adsorptive balance of dye on all samples could be achieved in the first 15 min of the process. Based on this result, the time for adding H_2O_2 in the further tests was selected to be 15 min after the addition of MO into reaction solution. The difference in the adsorption capacities of three samples is not significant. After reaching equilibrium, about 34%, 30% and 28% of MO were adsorbed on Fe_2MnO_4/AC-H, Fe_3O_4/AC-H and AC-H, respectively. Although the Fe_2MnO_4/AC-H has a lower porosity as compared to the Fe_3O_4/AC-H, its adsorption capacity is higher than that of Fe_3O_4/AC-H. This can be associated with their pH_{PZC}. pH_{PZC} of the Fe_2MnO_4/AC-H was 9.9 (Table 1), higher than that of Fe_3O_4/AC-H (9.0) and so at pH 4, the Fe_2MnO_4/AC-H exhibited higher positive surface charge compared to the Fe_3O_4/AC-H. Thus it attracted the $C_{14}H_{14}N_3O_3S^-$ anions stronger.

Table 2
The magnetic property of Fe_3O_4/AC-H and Fe_2MnO_4/AC-H samples.

Sample	Hc (Oe)	Mr (emu g^{-1})	Ms (emu g^{-1})
Fe_3O_4/AC-H	108	1.1	6.2
Fe_2MnO_4/AC-H	108	0.85	6.2

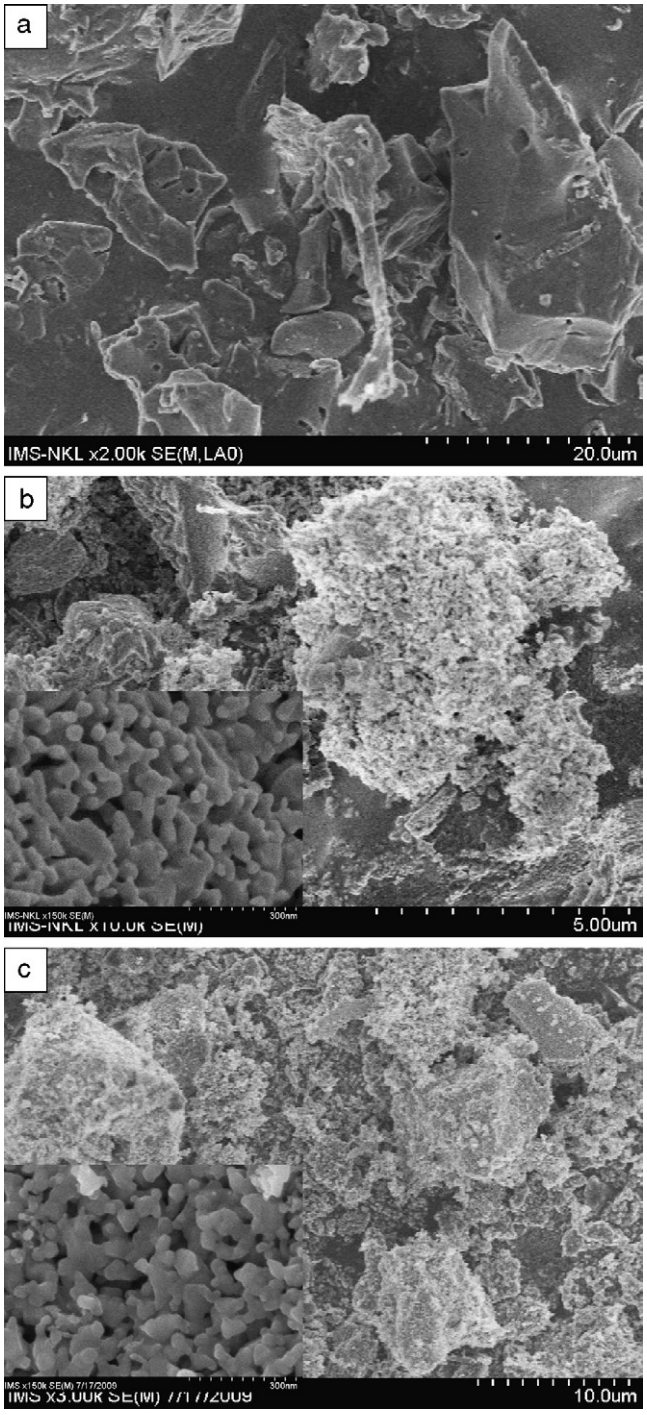

Fig. 4. SEM images of (a) AC-H, (b) Fe_3O_4/AC-H and (c) Fe_2MnO_4/AC-H. The inset shows the higher resolution images.

The removal of MO by adsorption and oxidation on the Fe_2MO_4/AC-H with H_2O_2 is shown in Fig. 7. For AC-H, the MO elimination is mainly attributed to the adsorption, but in the case of Fe_2MnO_4/AC-H and Fe_3O_4/AC-H, it is mainly attributed to the catalytic degradation. The Fe_2MnO_4/AC-H has a much higher MO degradation efficiency compared to the Fe_3O_4/AC-H. The Fe_2MnO_4/AC-H exhibited 100% MO degradation efficiency within 90 min of reaction (after adding H_2O_2) while the degrada-

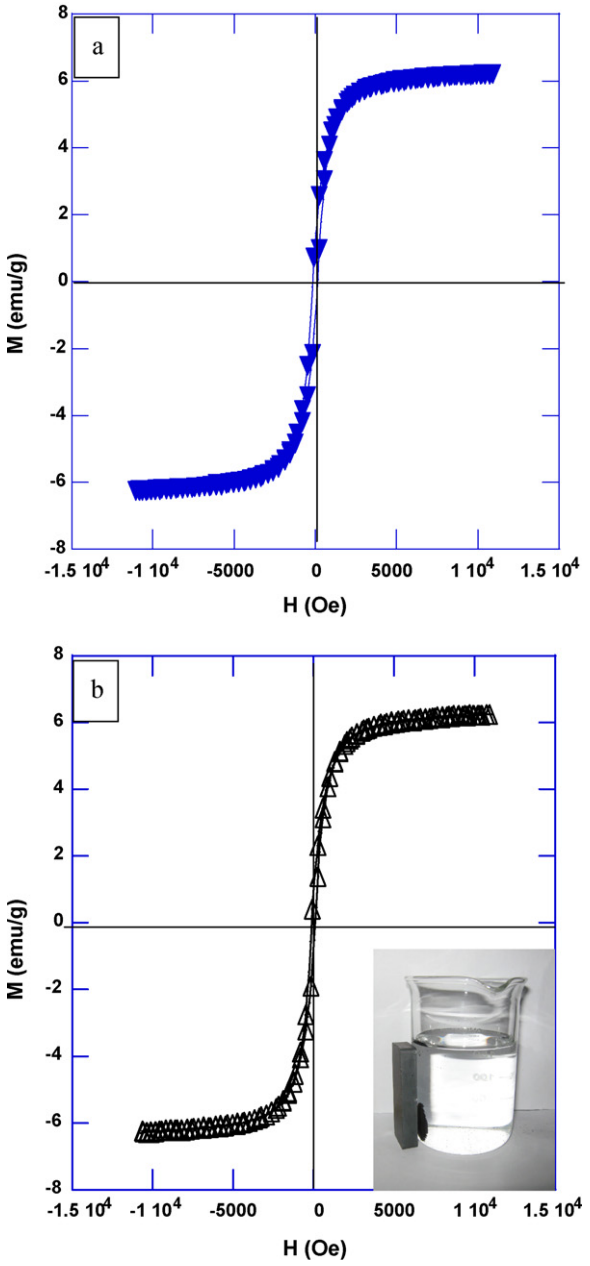

Fig. 5. Hysteresis loops of (a) Fe_3O_4/AC-H and (b) Fe_2MnO_4/AC-H samples, the inset shows photograph of the sample attracted by a magnet.

tion efficiency of Fe_3O_4/AC-H was 55%. However, the low activity of Fe_3O_4/AC-H may not be solely attributed to low or high iron loading because, in fact, we prepared Fe_3O_4/AC-H samples with low iron loading (1.6 wt% and 2.6 wt%) and with relatively high iron loading (5 wt% and 9 wt%) obtained by using the impregnation with heating at 100 °C to remove water vapor are still lower than that of Fe_2MnO_4/AC-H. After 90 min of reaction, only about 46%, 51%, 56% and 58% of MO were degraded by Fe_3O_4/AC-H with 1.6 wt%, 2.6 wt%, 5 wt% and 9 wt% of Fe, respectively. The reason for the increase in activity of the Fe_2MnO_4/AC-H for the Fenton reaction is not yet clear, but may be explained by possible electron transfer processes within the Fe_2MnO_4 particles during the reaction [26,27]. According to Costa et al. [26,27] the reduction of Mn^{3+} by Fe^{2+} is thermodynamically favourable as shown by the following equations:

$$Fe^{3+} + 1e^- \rightarrow Fe^{2+} \qquad E^0 = 0.77\,V \tag{1}$$

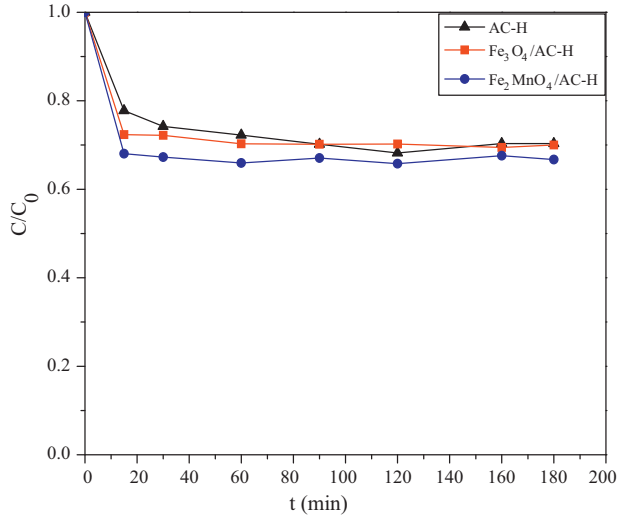

Fig. 6. MO removal by adsorption on AC-H, Fe_3O_4/AC-H and Fe_2MnO_4/AC-H samples. Experimental conditions: MO 50 mg L^{-1}, catalyst 2.5 g L^{-1}, T = 302.0 ± 1.0 K and pH 4.0 ± 0.1.

$$Mn^{3+} + 1e^- \rightarrow Mn^{2+} \qquad E^0 = 1.51\,V \tag{2}$$

$$Fe^{2+} + Mn^{3+} \rightarrow Fe^{3+} + Mn^{2+} \qquad E^0 = 0.73\,V \tag{3}$$

This reduction could take place by an electron transfer process within the semiconductor oxide structure. Magnetite is a high conductivity semiconductor with a narrow band gap (0.1 eV) with almost metallic character (ca. 10^2–$10^3\ \Omega^{-1}\,cm^{-1}$) [44,45] which is also important for electron transport. Therefore the efficient regeneration of the surface Mn^{2+} species by this process would be responsible for the remarkable increase an activity of H_2O_2 decomposition and organic oxidation.

3.3. Effect of pH

The effects of pH on the MO removal by both Fe_2MnO_4/AC-H and Fe_3O_4/AC-H were determined at a pH range of 3–7. The results obtained (Fig. 8) show that for both samples used, the MO

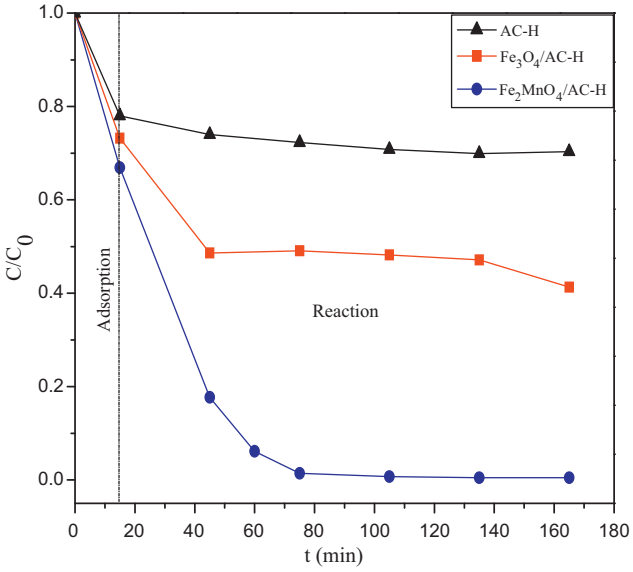

Fig. 7. MO removal by adsorption and oxidation on AC-H, Fe_3O_4/AC-H and Fe_2MnO_4/AC-H samples. Experimental conditions: MO 50 mg L^{-1}, H_2O_2 1.8×10^{-2} mol L^{-1}, catalyst 2.5 g L^{-1}, T = 302.0 ± 1.0 K and pH 4.0 ± 0.1.

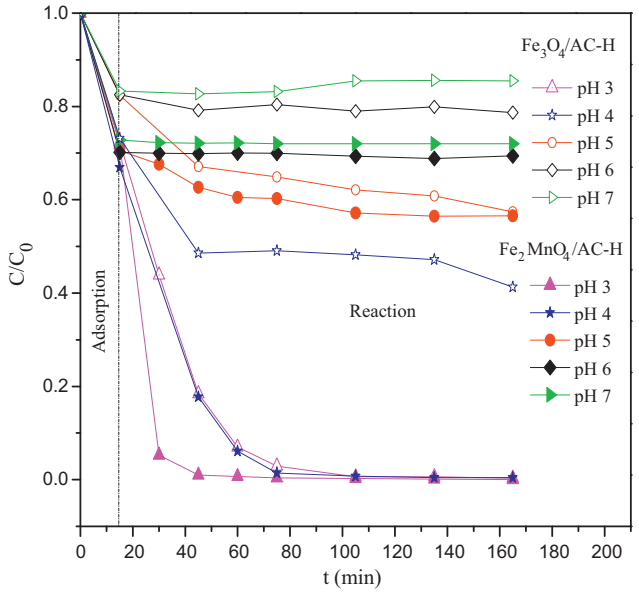

Fig. 8. pH effect on the degradation of MO solution using Fe_3O_4/AC-H and Fe_2MnO_4/AC-H. Experimental conditions: MO 50 mg L^{-1}, H_2O_2 1.8×10^{-2} mol L^{-1}, catalyst 2.5 g L^{-1} and $T = 302.0 \pm 1.0$ K.

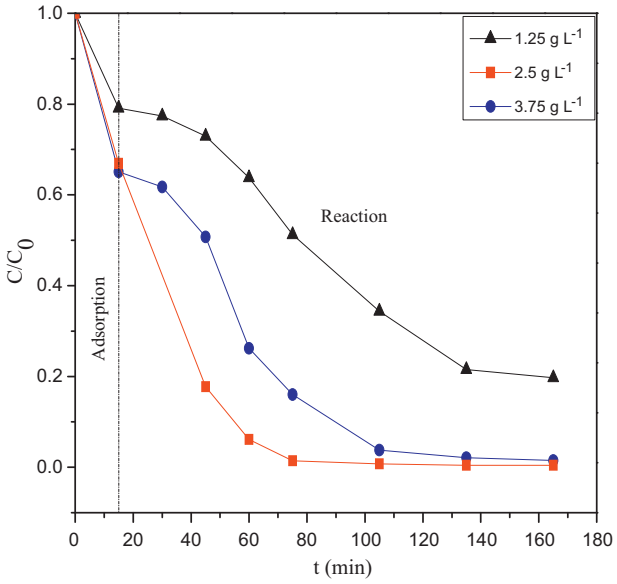

Fig. 9. The influence of Fe_2MnO_4/AC-H catalyst loading on the degradation of MO. Experimental conditions: MO 50 mg L^{-1}, H_2O_2 1.8×10^{-2} mol L^{-1}, $T = 302.0 \pm 1.0$ K and pH 4.0 ± 0.1.

removal decreases when increasing the pH. This observation is consistent with previously reported results [46,47]. In addition, the Fe_2MnO_4/AC-H catalyst is more active than the Fe_3O_4/AC-H one at any pH studied (between 3 and 7). For example, at pH 3, about 97% and 100% of MO are degraded by the Fe_3O_4/AC-H and Fe_2MnO_4/AC-H catalysts respectively after 60 min of reaction. Fig. 8 also shows the best results of the MO degradation for both catalysts at pH 3. However, for Fe_2MnO_4/AC-H catalyst, its catalytic activity is still kept up over pH 4. This is an important advantage because it is well known that one major drawback of homogeneous Fenton process is the narrow pH range (pH < 3) which is unfavourable in practice due to the costs of acidification during processing and neutralization after treatment. For these reasons, further experiments will be carried out at pH 4 using the most promising catalyst, Fe_2MnO_4/AC-H.

3.4. Effect of catalyst loading

The impact of Fe_2MnO_4/AC-H dosage on the degradation of MO was investigated in the range of 1.25–3.75 g L^{-1}. As shown in Fig. 9, the degradation efficiency increased with the catalyst dosage up to 2.5 g L^{-1}, and then slightly decreased upon further addition of the catalyst. The same phenomenon has been reported by Liao et al. [48]. The inhibition effect of iron and manganese species is considered as the reason for this decrease because the scavenging of hydroxyl radicals or other radicals will occur when presenting excessive metal species, which can be expressed by the following equations [48–51].

$$\equiv M^{II} + {}^{\bullet}OH \rightarrow \equiv M^{III} + OH^{-} \quad (M: Fe \text{ or } Mn) \tag{4}$$

$$\equiv M^{II} + {}^{\bullet}OOH \rightarrow \equiv M^{III} + OOH^{-} \tag{5}$$

3.5. Effect of H_2O_2 dosage

Fig. 10 shows the effect of H_2O_2 dosage in the range of 5.0×10^{-3}–3.7×10^{-2} mol L^{-1} on the degradation of MO. The degradation efficiency of MO increased with increasing concentrations of H_2O_2 from 5.0×10^{-3} mol L^{-1} to 1.8×10^{-2} mol L^{-1}. The enhancement of the degradation rate by addition of H_2O_2 is due to an increase in •OH radicals. However, it should be pointed out that when the concentration of H_2O_2 was over 1.8×10^{-2} mol L^{-1}, the degradation of MO decreased. This can be explained by the scavenging of •OH radicals at a higher H_2O_2 dosage, leading to a decrease in the number of •OH radicals in solution (Eqs. (6) and (7)) [52].

$$H_2O_2 + {}^{\bullet}OH \rightarrow H_2O + {}^{\bullet}OOH \tag{6}$$

$${}^{\bullet}OOH + {}^{\bullet}OH \rightarrow H_2O + O_2 \tag{7}$$

3.6. Effect of the initial MO concentration

The influence of various initial concentrations of MO on the degradation process was investigated between 30 mg L^{-1} and 60 mg L^{-1} MO solutions. The results obtained (Fig. 11) shown that the degradation rate is decreased by increasing initial concentrations as expected, because the increase in dye concentration will increase the number of dye molecules and competition with the number of •OH radicals in the solution. It should be noted that even at a high initial concentration of MO, for example,

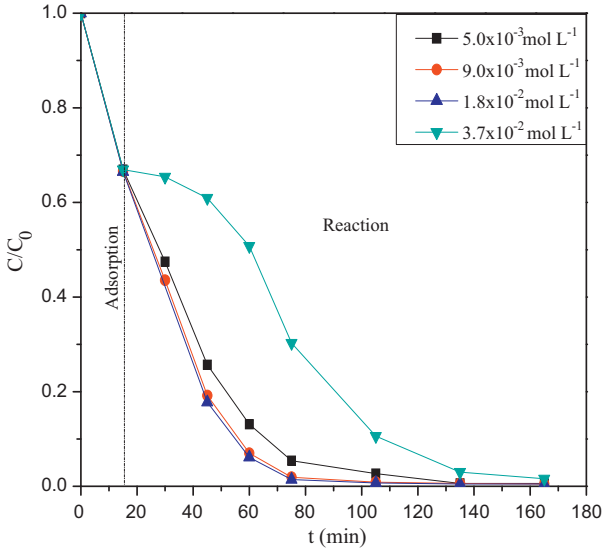

Fig. 10. Effect of H_2O_2 concentration on the degradation of MO. Experimental conditions: MO 50 mg L^{-1}, Fe_2MnO_4/AC-H 2.5 g L^{-1}, $T = 302.0 \pm 1.0$ K and pH 4.0 ± 0.1.

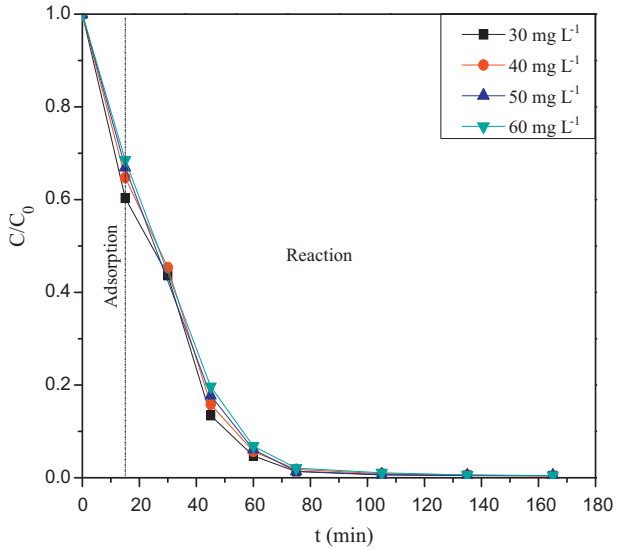

Fig. 11. Effect of the initial-concentration of MO on the degradation rate. Experimental conditions: H_2O_2 1.8×10^{-2} mol L^{-1}, Fe_2MnO_4/AC-H 2.5 g L^{-1}, $T = 302.0 \pm 1.0$ K and pH 4.0 ± 0.1.

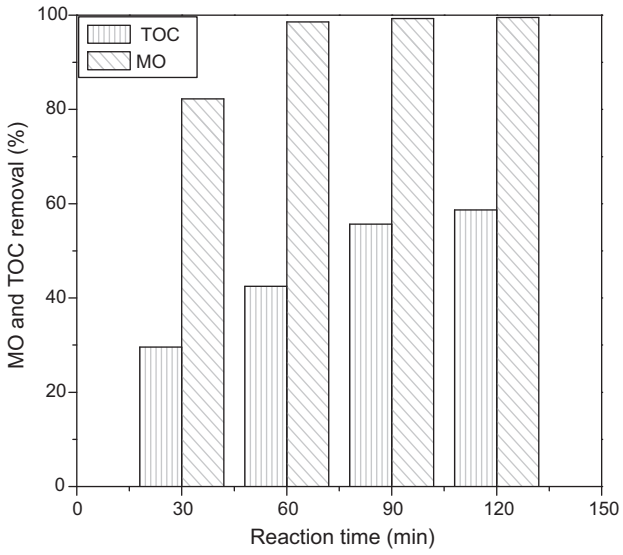

Fig. 13. Comparison of MO and TOC removal of 50 mg L^{-1} MO obtained using 2.5 g L^{-1} Fe_2MnO_4/AC-H and 1.8×10^{-2} mol L^{-1} H_2O_2 at $T = 302.0 \pm 1.0$ K and pH 4.0 ± 0.1.

60 mol L^{-1}, the degradation can also be achieved at about 100% after 90 min.

3.7. The analysis of reaction products in degradation process

The absorption spectra of MO were scanned in the range 190–700 nm, as given in Fig. 12. Regarding the MO spectrum, it is characterized by one band in the ultraviolet region located at 270 nm and by one band in the visible region located at 465 nm. The UV band is attributed to the $\pi \rightarrow \pi^*$ transition of the aromatic rings in the MO molecule is the characteristic of two adjacent rings, whereas the band in the visible region originates from a conjugated structure formed by the azo bond under the strong influence of the electron-donating dimethylamino group [53]. Obviously, both bands located at 465 and 270 nm decreased rapidly following reaction time and tended to disappear after 120 min of reaction, without the appearance of new adsorption bands in the visible region. This reflects that the degradation of the MO was practically complete. However, the spectrum in the range of 190–250 nm shows that the MO was not completely mineralized, even though the absorption intensity was reduced within the range. The conclusion was further confirmed by TOC result. As shown in Fig. 13, the TOC reduction was significantly lower than MO degradation. After 120 min the MO degradation reached 100% while the TOC reduction only reached around 59%. The result implies that significant amounts of intermediates still remain in the solution.

3.8. Stability and reuse of catalyst

Fig. 14 shows the MO degradation on the Fe_2MnO_4/AC-H in three consecutive experiments. Between each experiment, the catalyst was separated from the solution by filtration, washed with deionized water, and dried at 100 °C over night. It is seen that the initial catalytic activity of Fe_2MnO_4/AC-H decreased gradually during these three runs. This initial loss of activity may be

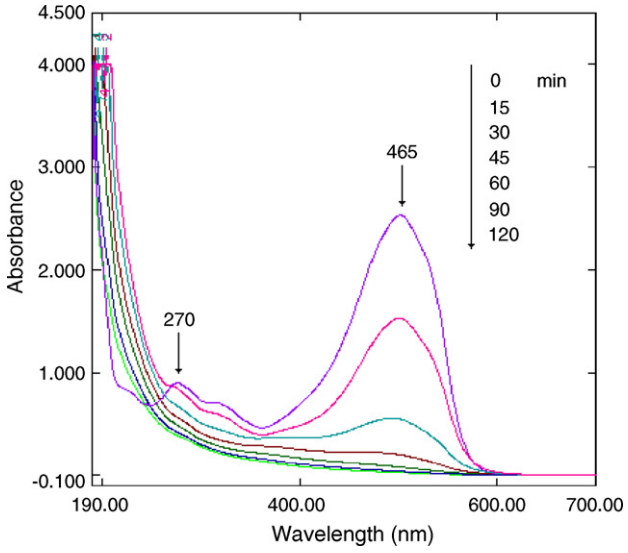

Fig. 12. UV–vis spectral changes of the 50 mg L^{-1} MO solution in degradation process as a function of reaction time in the presence of 2.5 g L^{-1} Fe_2MnO_4/AC-H, 1.8×10^{-2} mol L^{-1} H_2O_2 at $T = 302.0 \pm 1.0$ K and pH 4.0 ± 0.1.

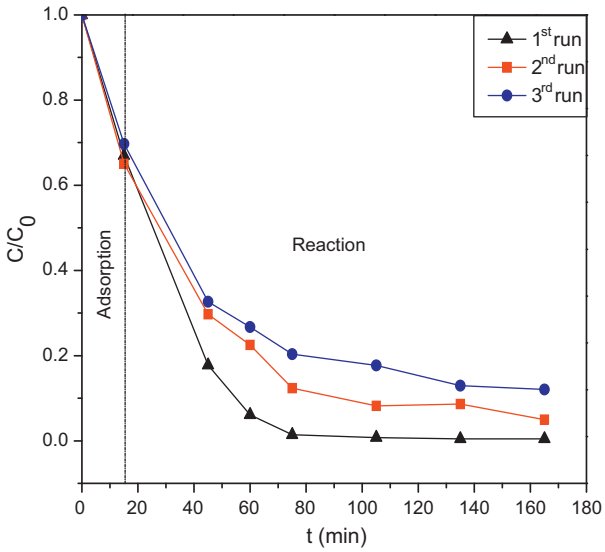

Fig. 14. Reuse of catalyst. Experimental conditions: MO 50 mg L^{-1}, H_2O_2 1.8×10^{-2} mol L^{-1}, Fe_2MnO_4/AC-H 2.5 g L^{-1}, $T = 302.0 \pm 1.0$ K and pH 4.0 ± 0.1.

due to the difficulty in completely removing residual by-products and reactants from active catalytic sites using the washing and drying processes. The catalyst deactivation can also be explained by the decay of active catalytic sites caused by small amounts of leached iron and manganese from the catalyst surface [10,54,55]. The concentrations of leached iron and manganese after each recycling were found to be about 0.47 mg L^{-1}, 0.30 mg L^{-1}, 0.26 mg L^{-1}, 0.22 mg L^{-1}, and 0.23 mg L^{-1} and 0.20 mg L^{-1}, which corresponds to around 0.71 wt%, 1.28 wt%, 0.26 wt%, 0.95 wt%, and 0.35 wt% and 0.87 wt% of the actual loss percentage of leached iron and manganese after each recycling, providing evidence for this explanation. However, when a mixture containing 0.5 mg L^{-1} Fe^{3+} and 0.5 mg L^{-1} Mn^{2+} ions was employed as a homogeneous catalyst for the Fenton reaction under the same condition, the MO was not significantly decomposed within 20 min. Therefore the MO degradation is considered as, essentially, a heterogeneous Fenton reaction. Further research is necessary to enlighten the causes of catalyst deactivation in order to diminish this problem and to develop some efficient regeneration procedure.

4. Conclusions

In summary, we have presented a simple and efficient method for the preparation of magnetic Fe_2MO_4 (M:Fe and Mn) activated carbons by impregnating the activated carbon with simultaneous magnetic precursor and carbon modifying agent followed by calcinations. The obtained magnetic activated carbons thus exhibit high surface areas and porosities and can be manipulated easily by an external magnetic field. The Fe_2MnO_4/AC-H exhibited enhanced activity in Fenton oxidation of methyl orange compared with the Fe_3O_4/AC-H sample. It was found that 100% degradation and 59% TOC removal of 50 mg L^{-1} MO could be achieved by using Fe_2MnO_4/AC-H in 120 min of reaction. Stability of the catalyst was demonstrated in up to three consecutive experiments showing that the reaction is essentially heterogeneous. An additional advantage of this method is using HNO_3 as a carbon modifying agent which is possible to functionalize the carbon surface by forming carboxyl groups [56–59] and these magnetic activated carbons thus could be used for advanced applications in areas such as the fabrication of high performance catalysts or the selective separation of biomolecules. On the other hand, the modification also makes binding between the magnetic particles and carbon become stronger. This may be a reason for low Fe and Mn leaching.

Acknowledgments

The authors acknowledge the National Foundation for Science & Technology Development of Viet Nam, (NAFOSTED) for their financial support of this work. Special gratitude to Mr. Thanh Son Cu and Mr. Manh Duong Nguyen for their technical support during XRD experiments and Nitrogen Adsorption Isotherm experiments.

References

[1] Y.L. Song, J.T. Li, Degradation of C.I. Direct Black 168 from aqueous solution by fly ash/H_2O_2 combining ultrasound, Ultrason. Sonochem. 16 (2009) 440–444.
[2] E.V. Kuznetsova, E.N. Savinov, L.A. Vostrikova, V.N. Parmon, Heterogeneous catalysis in the Fenton-type system FeZSM-5/H_2O_2, Appl. Catal. B: Environ. 51 (2004) 165–170.
[3] S. Caudo, G. Centi, C. Genovese, S. Perathoner, Homogeneous versus heterogeneous catalytic reactions to eliminate organics from waste water using H_2O_2, Top. Catal. 40 (2006) 207–219.
[4] E. Neyens, J. Baeyens, A review of classic Fenton's peroxidation as an advanced oxidation technique, J. Hazard. Mater. 98 (2003) 33–50.
[5] G. Centi, S. Perathoner, T. Torre, M.G. Verduna, Catalytic wet oxidation with H_2O_2 of carboxylic acids on homogeneous and heterogeneous Fenton-type catalysts, Catal. Today 55 (2000) 61–69.
[6] K. Fajerwerg, T. Castan, J.N. Foussard, A. Perrard, H. Debellefontaine, Influence de quelques paramètres opératoires sur l'oxydation du phénol par le peroxyde d'hydrogène en présence d'une zéolithe Fe-ZSM-5 dependency on some operating parameters during wet oxidation of phenol by hydrogen peroxide with Fe-ZSM-5 Zeolite, Environ. Technol. 21 (2000) 337–344.
[7] G. Centi, P. Ciambelli, S. Perathoner, P. Russo, Environmental catalysis: trends and outlooks, Catal. Today 75 (2002) 3–15.
[8] S. Perathoner, G. Centi, Wet hydrogen peroxide catalytic oxidation (WHPCO) of organic waste in agro-food and industrial streams, Top. Catal. 33 (2005) 207–224.
[9] E.V. Kuznetsova, E.N. Savinov, L.A. Vostrikova, G.V. Echevskii, The catalytic and photocatalytic oxidation of organic substances using heterogeneous Fenton-type catalysts, Water Sci. Technol. 49 (2004) 109–116.
[10] M. Tekbas, H.C. Yatmaz, N. Bektas, Heterogeneous photo-Fenton oxidation of reactive azo dye solutions using iron exchanged zeolite as a catalyst, Microporous Mesoporous Mater. 115 (2008) 594–602.
[11] M.B. Kasiri, H. Aleboyeh, A. Aleboyeh, Degradation of Acid Blue 74 using Fe-ZSM5 zeolite as a heterogeneous photo-Fenton catalyst, Appl. Catal. B: Environ. 84 (2008) 9–15.
[12] J. Guo, M. Al-Dahhan, Catalytic wet oxidation of phenol by hydrogen peroxide over pillared clay catalyst, Ind. Eng. Chem. Res. 42 (2003) 2450–2460.
[13] J. Feng, X. Hu, P.L. Yue, Effect of initial solution pH on the degradation of Orange II using clay-based Fe nanocomposites as heterogeneous photo-Fenton catalyst, Water Res. 40 (2006) 641–646.
[14] J. Chen, L. Zhu, Heterogeneous UV-Fenton catalytic degradation of dyestuff in water with hydroxyl-Fe pillared bentonite, Catal. Today 126 (2007) 463–470.
[15] M.A.D. León, J. Castiglioni, J. Bussi, M. Sergio, Catalytic activity of an iron-pillared montmorillonitic clay mineral in heterogeneous photo-Fenton process, Catal. Today 133–135 (2008) 600–605.
[16] Q. Chen, P. Wu, Y. Li, N. Zhu, Zh. Dang, Heterogeneous photo-Fenton photodegradation of reactive brilliant orange X-GN over iron-pillared montmorillonite under visible irradiation, J. Hazard. Mater. 168 (2009) 901–908.
[17] J. Jose, M. John, M.G. Gigimol, B. Mathew, Synthesis, characterization, and catalytic activity of crosslinked poly(*N*-vinyl-2-pyrrolidone acrylic acid) copolymer–metal complexes, J. Appl. Polym. Sci. 90 (2003) 895–904.
[18] P. Baldrian, T. Cajthaml, V. Merhautová, J. Gabriel, F. Nerud, P. Stopka, M. Hrubý, M.J. Beneš, Degradation of polycyclic aromatic hydrocarbons by hydrogen peroxide catalyzed by heterogeneous polymeric metal chelates, Appl. Catal. B 59 (2005) 267–274.
[19] W.Z. Tang, R.Z. Chen, Decolorization kinetics and mechanisms of commercial dyes by H_2O_2/iron powder system, Chemosphere 32 (1996) 947–958.
[20] A. Kornmuller, S. Karcher, M. Jekel, Adsorption of reactive dyes to granulated iron hydroxide and its oxidative regeneration, Water Sci. Technol. 46 (2002) 43–50.
[21] A.H. Gemeay, I.A. Mansour, R.G. El-Sharkawy, A.B. Zaki, Kinetics and mechanism of the heterogeneous catalyzed oxidative degradation of indigo carmine, J. Mol. Catal. A: Chem. 193 (2003) 109–120.
[22] A.H. Gemeay, I.A. Mansour, R.G. El Sharkawy, A.B. Zaki, Catalytic effect of supported metal ion complexes on the induced oxidative degradation of pyrocatechol violet by hydrogen peroxide, J. Colloid Interface Sci. 263 (2003) 228–236.
[23] B.W. Tyre, R.J. Watts, G.C. Miller, Treatment of four biorefractory contaminants in soils using catalyzed hydrogen peroxide, J. Environ. Qual. 20 (1991) 832–838.
[24] S.H. Kong, R.J. Watts, J.H. Choi, Treatment of petroleum-contaminated soils using iron mineral catalyzed hydrogen peroxide, Chemosphere 37 (1998) 1473–1482.
[25] W.P. Kwan, B.M. Voelker, Rates of hydroxyl radical generation and organic compound oxidation in mineral-catalyzed Fenton-like systems, Environ. Sci. Technol. 37 (2003) 1150–1158.
[26] R.C.C. Costa, M. de Fatima, F. Lelis, L.C.A. Oliveira, J.D. Fabris, J.D. Ardisson, R. Rios, C.N. Silva, R.M. Lago, Remarkable effect of Co and Mn on the activity of $Fe_{3-x}M_xO_4$ promoted oxidation of organic contaminants in aqueous medium with H_2O_2, Catal. Commun. 4 (2003) 525–529.
[27] R.C.C. Costa, M.F.F. Lelis, L.C.A. Oliveira, J.D. Fabris, J.D. Ardisson, R. Rios, C.N. Silva, R.M. Lago, Novel active heterogeneous Fenton system based on $Fe_{3-x}M_xO_4$ (Fe, Co, Mn, Ni): The role of M^{2+} species on the reactivity towards H_2O_2 reactions, J. Hazard. Mater. 129 (2006) 171–178.
[28] S.R. Rudge, T.L. Kurtz, C.R. Vessely, L.G. Catterall, D.L. Williamson, Preparation, characterization, and performance of magnetic iron–carbon composite microparticles for chemotherapy, Biomaterials 21 (2000) 1411–1420.
[29] A.B Fuertes, P. Tartaj, A facile route for the preparation of superparamagnetic porous carbons, Chem. Mater. 18 (2006) 1675–1679.
[30] I. Safarik, K. Nymburska, M. Safarikova, Adsorption of water-soluble organic dyes on magnetic charcoal, J. Chem. Technol. Biotechnol. 69 (1997) 1–4.
[31] L.C.A. Oliveira, R.V.R.A. Rios, J.D. Fabris, V. Garg, K. Sapag, R.M. Lago, Activated carbon/iron oxide magnetic composites for the adsorption of contaminants in water, Carbon 40 (2002) 2177–2183.
[32] G. Zhang, J. Qu, H. Liu, A.T. Cooper, R. Wu, $CuFe_2O_4$/activated carbon composite: a novel magnetic adsorbent for the removal of acid orange II and catalytic regeneration, Chemosphere 68 (2007) 1058–1066.
[33] J. Feng, X. Hu, P.L. Yue, Discoloration and mineralization of orange II using different heterogeneous catalysts containing Fe: a comparative study, Environ. Sci. Technol. 38 (2004) 5773–5778.
[34] IUPAC Recommendations, Reporting physisorption data for gas/solid systems with special reference to the determination of surface area and porosity, Pure Appl. Chem. 57 (1985) 603–619.

[35] S. Lowell, J.E. Shields, M.A. Thomas, M. Thommes, Characterization of Porous Solids And Powders: Surface Area Pore Size And Density, Kluwer Academic Publishers, Amsterdam, 2004, 13-45.
[36] G. Hermann, K. Huttinger, Mechanism of iron-catalyzed water vapour gasification of carbon, Carbon 24 (1986) 429–435.
[37] J.L. Figueiredo, J. Rivera-Utrilla, M.A. Ferro-Garcia, Gasification of active carbons of different texture impregnated with nickel, cobalt and iron, Carbon 25 (1987) 703–708.
[38] J.J Freeman, F.G.R. Gimblett, K.S.W. Sing, Studies of activated charcoal cloth. V. Modification of pore structure by impregnation with certain transition metal salts and oxo-complexes, Carbon 27 (1989) 85–93.
[39] A. Albiniak, D. Begin, E. Alain, G. Furdin, E. Broniek, J. Kaczmarczyk, Effect of iron enrichment with GIC or $FeCl_3$ on the pore structure and reactivity of coking coal, Fuel 76 (1997) 1383–1387.
[40] J. Alcañiz-Monge, M.A. Lillo-Ródenas, A. Bueno-López, M.J. Illán-Gómez, The influence of iron chloride addition to the precursor pitch on the formation of activated carbon fibers, Microporous Mesoporous Mater. 100 (2007) 202–209.
[41] L.C.A. Oliveira, E. Pereira, I.R. Guimaraes, A. Vallone, M. Pereira, J.P. Mesquita, K. Sapag, Preparation of activated carbons from coffee husks utilizing $FeCl_3$ and $ZnCl_2$ as activating agents, J. Hazard. Mater. 165 (2009) 87–94.
[42] T. Yang, Ch. Shen, Z. Li, H. Zhang, C. Xiao, Sh. Chen, Zh. Xu, D. Shi, J. Li, H. Gao, Highly ordered self-assembly with large area of Fe_3O_4 nanoparticles and the magnetic properties, J. Phys. Chem. B 109 (2005) 23233–23236.
[43] O. Masala, R. Seshadri, Magnetic properties of capped, soluble $MnFe_2O_4$ nanoparticles, Chem. Phys. Lett. 402 (2005) 160–164.
[44] A.J. Bard, J.K. Leland, Photochemistry of colloidal semiconducting iron oxide polymorphs, J. Phys. Chem. 91 (1987) 5076–5083.
[45] A.F. White, Heterogeneous electrochemical reactions associated with oxidation of Ferrous oxide and silicate surfaces, Rev. Miner. 23 (1990) 467–509.
[46] S. Parra, L. Henao, E. Mielczarski, J. Mielczarski, P. Albers, E. Suvorova, J. Guindet, J. Kiwi, Synthesis, testing, and characterization of a novel Nafion membrane with superior performance in photoassisted immobilized Fenton catalysis, Langmuir 20 (2004) 5621–5629.
[47] S. Parra, I. Guasaquillo, O. Enea, E. Mielczarski, J. Mielczarki, P. Albers, L. Kiwi-Minsker, J. Kiwi, Abatement of an azo dye on structured C-Nafion/Fe-ion surfaces by photo-Fenton reactions leading to carboxylate intermediates with a remarkable biodegradability increase of the treated solution, J. Phys. Chem. B 107 (2003) 7026–7035.
[48] Q. Liao, J. Sun, L. Gao, Degradation of phenol by heterogeneous Fenton reaction using multi-walled carbon nanotube supported Fe_2O_3 catalysts, Colloids Surf. A: Physicochem. Eng. Aspects 345 (2009) 95–100.
[49] A. Romero, A. Santos, F. Vicente, Chemical oxidation of 2,4-dimethylphenol in soil by heterogeneous Fenton process, J. Hazard. Mater. 162 (2009) 785–790.
[50] J.H. Ramirez, F.J. Maldonado-Hódar, A.F. Pérez-Cadenas, C. Moreno-Castilla, C.A. Costa, L.M. Madeira, Azo-dye Orange II degradation by heterogeneous Fenton-like reaction using carbon-Fe catalysts, Appl. Catal. B: Environ. 75 (2007) 312–323.
[51] S.W. Lam, K. Chiang, T.M. Lim, R. Amal, G.K.-C. Low, The role of ferric ion in the photochemical and photocatalytic oxidation of resorcinol, J. Catal. 234 (2005) 292–299.
[52] S. Parra, V. Nadtotechenko, P. Albers, J. Kiwi, Discoloration of azo-dyes at biocompatible pH-values through an Fe-histidine complex immobilized on Nafion via Fenton-like processes, J. Phys. Chem. B 108 (2004) 4439–4448.
[53] J. Fan, Y. Guo, J. Wang, M. Fan, Rapid decolorization of azo dye methyl orange in aqueous solution by nanoscale zerovalent iron particles, J. Hazard. Mater. 166 (2009) 904–910.
[54] J.H. Ramirez, C.A. Costa, L.M. Madeira, G. Mata, M.A. Vicente, M.L.R. Cervantes, A.J.L. Peinado, R.M.M. Aranda, Fenton-like oxidation of Orange II solutions using heterogeneous catalysts based on saponite clay, Appl. Catal. B: Environ. 71 (2007) 44–56.
[55] J. Deng, J. Jiang, Y. Zhang, X. Lin, Ch. Du, Y. Xiong, $FeVO_4$ as a highly active heterogeneous Fenton-like catalyst towards the degradation of Orange II, Appl. Catal. B: Environ. 84 (2008) 468–473.
[56] C.L. Mangun, K.R. Benak, J. Economy, K.L. Foster, Surface chemistry, pore sizes and adsorption properties of activated carbon fibers and precursors treated with ammonia, Carbon 39 (2001) 1809–1820.
[57] L. Li, P.A. Quinlivan, D.R.U. Knappe, Effects of activated carbon surface chemistry and pore structure on the adsorption of organic contaminants from aqueous solution, Carbon 40 (2002) 2085–2100.
[58] S.H. Wu, P. Pendleton, Adsorption of anionic surfactant by activated carbon: effect of surface chemistry, ionic strength, and hydrophobicity, J. Colloid Interface Sci. 243 (2001) 306–315.
[59] M.F.R. Pereira, S.F. Soares, J.J.M. Orfao, J.L. Figueiredo, Adsorption of dyes on activated carbons: influence of surface chemical groups, Carbon 41 (2003) 811–821.